



Full length article

An electrochemical outlook upon the gaseous ethanol sensing by graphene oxide-SnO₂ hybrid materials



E. Pargoletti^{a,b,*}, A. Tricoli^c, V. Pifferi^{a,b}, S. Orsini^a, M. Longhi^{a,b}, V. Guglielmi^{a,b}, G. Cerrato^d, L. Falciola^{a,b}, M. Derudi^e, G. Cappelletti^{a,b}

^a Dipartimento di Chimica, Università degli Studi di Milano, via Golgi 19, 20133 Milano, Italy

^b Consorzio Interuniversitario Nazionale per la Scienza e Tecnologia dei Materiali (INSTM), Via Giusti 9, 50121 Firenze, Italy

^c Nanotechnology Research Laboratory, College of Engineering and Computer Science, The Australian National University, Canberra ACT 2601, Australia

^d Dipartimento di Chimica and NIS, Inter-department Center, Università di Torino, Via Giuria 7, 10125 Torino, Italy

^e Dipartimento di Chimica, Materiali e Energia Chimica “Giulio Natta”, Politecnico di Milano, Via Mancinelli 7, 20131 Milano, Italy

ARTICLE INFO

Keywords:

Tin dioxide
Graphene oxide
Ethanol
Gas sensor
Electron transfer
Low temperature

ABSTRACT

Breakthroughs in the synthesis of hybrid materials have led to the development of a plethora of chemiresistors that could operate at lower and lower temperatures. Herein, we report the fabrication of novel composite materials (SnO₂-GO 4:1, 8:1 and 16:1) based on graphene oxide (GO) sheets decorated with tin dioxide nanoparticles, through a controlled chemical growth. We succeeded in obtaining widely spaced isles of the metal oxide on the carbonaceous material, thus enhancing the electron transfer process (*i.e.* favored convergent diffusion, as investigated through cyclic voltammetric analysis), which plays a pivotal role for the final sensing behavior. Indeed, only with SnO₂-GO 16:1 sample, superior responses towards gaseous ethanol were observed both at 150 °C and at RT (by exploiting the UV light), with respect to pristine SnO₂ and mechanically prepared SnO₂(16)@GO material. Particularly, an improvement of the sensitivity (down to 10 ppb), response and recovery times (about of 60–70 s) was assessed. Besides, all the powders were finely characterized on structural (XRPD, FTIR and Raman spectroscopies), surface (active surface area, pores volume, XPS), morphological (SEM, TEM) and electrochemical (cyclic voltammetries) points of view, confirming the effective growth of SnO₂ nanoparticles on the GO sheets.

1. Introduction

The sensing of ethanol plays a remarkable role in several fields, such as breath analysis [1], traffic safety [2] and food industries, especially in wine quality monitoring [3]. Currently, among the most exploited gas sensors, chemiresistors made of metal oxide semiconductors (*e.g.* ZnO [4,5], SnO₂ [2,6], WO₃ [7,8] or In₂O₃ [9]) are deeply investigated. Especially, SnO₂ has attracted considerable attention due to its heat tolerance, low cost and superior sensing behavior towards several inorganic/organic gaseous species, thus showing very short response and recovery times (around 10 s) at high operating temperatures (above 200 °C) [10,11]. However, its main shortcomings are both the large power consumption and the selectivity [12,13]. Hence, in order to overcome the former, the reduction of the operating temperature may represent a valuable solution. In this context, the coupling of metal

oxides with graphene-based materials could play a pivotal role in solving the aforementioned issue [14]. Indeed, thanks to its high conductivity, it can improve the final sensing performances [15,16]. Zhang et al. stated that sensors based on ZnO/graphene hybrid materials can exhibit remarkably enhanced response towards acetone with respect to the pristine metal oxide [17]. Besides, Kalidoss et al. investigated a ternary composite based on GO, SnO₂ and TiO₂ and they have demonstrated this sensor can be a good candidate for the selective detection of acetone gas in breath of diabetes mellitus patients, at low operating temperatures [18].

Therefore, along with the achievement of more and more performing sensing devices, that could work at room temperatures, the mechanism underneath the sensor behavior is still a hot topic to be completely unraveled. In particular, concerning the composite graphene/metal oxides, a deep electrochemical characterization has not

* Corresponding author at: Università degli Studi di Milano, Dipartimento di Chimica, via Golgi 19, 20133 Milano, Italy.

E-mail addresses: eleonora.pargoletti@unimi.it (E. Pargoletti), antonio.tricoli@anu.edu.au (A. Tricoli), valentina.pifferi@unimi.it (V. Pifferi), silvia.orsini2@studenti.unimi.it (S. Orsini), mariangela.longhi@unimi.it (M. Longhi), vittoria.guglielmi@unimi.it (V. Guglielmi), giuseppina.cerrato@unito.it (G. Cerrato), luigi.falciola@unimi.it (L. Falciola), marco.derudi@polimi.it (M. Derudi), giuseppe.cappelletti@unimi.it (G. Cappelletti).

<https://doi.org/10.1016/j.apsusc.2019.04.046>

Received 3 December 2018; Received in revised form 27 March 2019; Accepted 4 April 2019

Available online 05 April 2019

0169-4332/ © 2019 Published by Elsevier B.V.

been reported so far, which may give a general comprehension of the synergistic effect between the two materials.

Hence, in the present work, the design and synthesis of SnO₂-based materials (either pristine or graphene oxide-based hybrids) have been studied, alongside with the sensing measurements towards low ethanol concentrations. Tests have been performed at temperatures lower than the commonly reported ones, by exploiting the UV light. Finally, a possible explanation of the significant differences seen in the sensing performances has been inferred through cyclic voltammetric analyses.

2. Material and methods

All the chemicals were of reagent-grade purity and were used without further purification; doubly distilled water passed through a Milli-Q apparatus was utilized. All the reagents used were purchased from Sigma-Aldrich.

2.1. Synthesis of hybrid SnO₂-GO compound

Graphene Oxide (GO) was prepared by adopting a modified Hummers' method, reported elsewhere [19,20].

For the synthesis of the composite materials, the appropriate amount of SnCl₄ × 5H₂O was dissolved in 3.0 mg mL⁻¹ of an aqueous GO suspension to have starting salt precursor-to-GO weight ratios equal to 4:1, 8:1 and 16:1. The mixture was stirred ($\omega = 300$ rpm) for 3 h at 50 °C and, then, 30 mL of stoichiometric urea aqueous solution (0.04, 0.10, 0.15 M) was added dropwise. The mixture was continuously stirred for other 3 h. Subsequently, the resultant product was centrifuged ($\omega = 8000$ rpm) several times with MilliQ water, until the pH became neutral. Then, it was dried in oven at 60 °C. A final calcination step at 400 °C, under oxygen flux (6 h, 9 NL h⁻¹) followed to form a greyish or whitish precipitate (according to the different coverage degree of the graphene oxide surface). For the sake of comparison, pure SnO₂ has been prepared through the same synthetic route.

Moreover, in order to have a corroboration of the effective controlled growth of tin dioxide particles on GO surface, XPS measurements were carried out and the relative Sn-to-C atomic ratios are reported in Table S1. For SnO₂-GO 16:1 sample, a value similar to the one determined for pristine SnO₂ was observed. Whereas, a lowering trend has been detected passing from SnO₂-GO 8:1 to 4:1, thus, a controlled decreasing of graphene oxide coverage by tin dioxide nanoparticles, as expected from the adopted synthetic procedure, is confirmed (Table S1, 2nd column).

2.2. Sample characterizations

X-Ray Powder Diffraction (XRPD) analyses were performed on a Philips PW 3710 Bragg-Brentano goniometer equipped with a scintillation counter, 1° divergence slit, 0.2 mm receiving slit and 0.04° Soller slit systems. We used graphite-monochromated Cu K α radiation (Cu K α_1 $\lambda = 1.54056$ Å, K α_2 $\lambda = 1.54433$ Å) at 40 kV × 40 mA nominal X-rays power. Diffraction patterns were collected between 20° and 90° with a step size of 0.1° and a total counting time of about 1 h. A microcrystalline Si-powder sample was employed as a reference to correct instrumental line broadening effects.

ATR-FTIR analyses were recorded between 4000 and 400 cm⁻¹ by means of Nicolet 380 Spectrophotometer-Thermo Electron Corporation.

Micro-Raman analyses have been performed by a Raman spectrometer equipped with a Jasco RMP-100 probe [21] provided with a narrow band interference filter to clean-up laser line and an edge filter to remove the Rayleigh scattering from sample, allowing to collect Raman spectra with a lower wavenumber limit of ~ 100 cm⁻¹. Scattered radiation was directed, by means of a 200 μ m core fiber, to an Oriel MS125 spectrometer. The Andor CCD detector (1024 × 128 pixel) was cooled by means of a Peltier device. The probe was also provided with an Olympus 50 × objective and an integrated video camera. The

laser source was a frequency-doubled Nd:YAG laser emitting at 532 nm and the power at the sample was around 1.5 mW. All the spectra were recorded between 2000 and 400 cm⁻¹ with a resolution estimated around 8 cm⁻¹ and were obtained as a sum of 20 accumulations with an exposure time of 4 s.

The BET surface area values, determined by a multipoint BET method, were acquired by Tristar II, Micromeritics. Before each analysis samples were pretreated at 150 °C for 4 h under a nitrogen flux. Desorption isotherms were used to determine the total pore volume using the Barrett-Joyner-Halenda (BJH) method.

Scanning Electron Microscopy (SEM) was carried out using a LEO 1430 Microscope (100 k × magnification, 5 nm resolution).

Transmission Electron Microscope (TEM) analyses were performed on LIBRA 200 EFTEM (Zeiss) instrument operated at 200 kV accelerating voltage. The TEM grids were prepared dropping the dispersed suspension of nanoparticles in isopropanol onto a holey-carbon supported copper grid and drying it in air at room temperature overnight.

X-Ray Photoelectron Spectroscopy (XPS) were obtained using a Mprobe apparatus (Surface Science Instruments). The source was the monochromatic Al K α radiation (1486.6 eV); a spot size of 200 × 750 nm and a pass energy of 25 eV were used. The 1s level of hydrocarbon-contaminant carbon was taken as the internal reference at 284.6 eV. The accuracy of the reported binding energies (B. E.) can be estimated to be around 0.2 eV and the resolution is equal to 0.74 eV.

Cyclic Voltammetry (CV) analyses were carried out on Glassy Carbon working electrode, modified by drop casting (20 μ L) of 0.5 mg mL⁻¹ dimethylformamide powders (*i.e.* pure SnO₂, SnO₂-GO 16:1 and SnO₂ mechanically mixed to GO with a corresponding ratio of about 16-to-1) suspensions. The electrochemical measurements were performed in a conventional three-electrode cell using a platinum foil as the counter electrode and a Saturated Calomel Electrode (SCE) as the reference one ($E = 0.244$ V vs SHE). A phosphate buffered saline solution (PBS) 0.1 M, at fixed pH 7.4, was utilized as the supporting electrolyte. Tests have been also performed by adding [Ru(NH₃)₆]Cl₃ probe or pure liquid ethanol to have a final concentration in PBS equal to 3 mM and 1 mM, respectively. The CVs were recorded at room temperature by using an Autolab PGStat30 (Ecochemie, The Netherlands) potentiostat/galvanostat controlled by NOVA 2.0 software for data acquisition. A step potential of 0.005 V and a scan rate of 0.1 V s⁻¹ were adopted, in the potential range between -2.0 and +2.0 V or -0.7 and +0.2 V (SCE).

2.3. Materials deposition on Pt-interdigitated electrodes (Pt-IDEs)

Powders were deposited on glass substrates topped with interdigitated Pt electrodes (Pt-IDEs) by a simple hot-spray method. The IDEs were made of glass on which interdigitated Pt lines with 5 μ m in width and space have been deposited (G-IDEAU5, DropSens, Oviedo, Spain) [22]. To remove any contamination from the electrodes, all substrates were sintered at 300 °C for 12 h and washed by several washing (ethanol)/drying cycles before deposition. Then, 4.0 mL of 2.5 mg mL⁻¹ ethanol powders suspensions were sprayed by keeping constant the air-brush pressure (0.8 bar), the temperature of the heating plate (230 °C) and the deposition height (8 cm). A final calcination step at 350 °C for 1 h was performed to guarantee a good powders film adhesion on IDEs. Therefore, the tested IDEs were prepared by adopting pristine SnO₂, hybrid material (*i.e.* SnO₂-GO 4:1, 8:1 and 16:1) and by spraying SnO₂ onto GO (*i.e.* SnO₂(16)@GO to compare to SnO₂-GO 16:1, the only ratio that guarantees an almost complete coverage of the graphene oxide layer).

2.4. Gas sensing tests

For gaseous ethanol sensing, O₂ (BOC Ltd) and N₂ (BOC Ltd) were controlled by mass flow controller (Bronkhorst), with a total gas flow rate of 0.5 L min⁻¹. The target gas (10 ppm in N₂, Coregas) were diluted

to 1 ppm and lower concentrations by using the simulated air ($0.1 \text{ L min}^{-1} \text{ O}_2 + 0.4 \text{ L min}^{-1} \text{ N}_2$, BOC Ltd.) before purging into the chamber, keeping constant the total flow rate. The temperature of the hotplate in the gas sensing chamber (Linkam) was controlled by a temperature controller and it was set at two different values (25 and 150°C). Every test was performed by exploiting the UV light. Therefore, the samples were illuminated through a quartz window by a solar simulator (NewSpec, LCS-100) with an FGUV5-UV – $\varnothing 25 \text{ mm}$ UG5 Colored Glass Filter (AR Coated: 290–370 nm, Thorlabs Inc.). For the gas sensing tests, two gold probes were separately placed on top of the powders covered IDEs, and the dynamic response was recorded by an electrochemical workstation (CHI 660E, USA) by applying a bias of $+1.0 \text{ V}$. The sensor response is reported as: $(R_{\text{air}}/R_{\text{analyte}}) - 1$, where R_{air} is the film resistance in air and R_{analyte} is the film resistance at a given concentration of the target gas [23]. Both sensors response and recovery times have been evaluated considering the 90% of the final response.

3. Results and discussion

3.1. Materials sensing response towards gaseous ethanol

The tin oxide sensing performances towards gaseous ethanol molecules has been widely reported, already showing good results. However, herein, the significant step forward consists in the amplification of the final signal, obtained with the hybrid $\text{SnO}_2\text{-GO}$ 16:1 material, giving the possibility to reach very low VOC concentrations, even at room temperature.

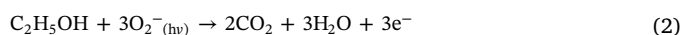
Fig. 1a–c compare the responses achieved increasing the GO surface coverage by tin dioxide (from 4:1 Sn salt precursor-to-GO weight ratio to 16:1). Indeed, as further corroborated by XPS measurements, the SnO_2 content rises passing from $\text{SnO}_2\text{-GO}$ 4:1 sample to 16:1, with respect to the underneath carbon material (Table S1). All the as-synthesized powders were tested either at 150°C or at room temperature, in both cases by exploiting the UV light. Hence, Figs. 1a–c and S1 show the response to 1 ppm or lower concentrations of gaseous ethanol for all the hybrid compounds. Although, the signal intensities seem to be good at 25°C only for $\text{SnO}_2\text{-GO}$ 8:1 and 16:1 (Fig. S1b and c), the greatest sensitivities were achieved at 150°C . Specifically, with $\text{SnO}_2\text{-GO}$ 16:1 a very good signal was obtained even down to 10 ppb (inset of Fig. 1c), having an optimal linear correlation between the sensor response intensities and the ethanol concentrations (Fig. 1f, green line).

Therefore, since the most promising results were acquired at 150°C , this experimental parameter was chosen for the subsequent tests. Actually, for the sake of clarity, pristine SnO_2 and SnO_2 sprayed on GO ($\text{SnO}_2(16)\text{@GO}$) were tested to enlighten the role played by graphene oxide-metal oxide chemical junction. Thus, as shown in Fig. 1d, pure tin dioxide gives a good signal only by purging ethanol with a concentration of 8 ppm. On the contrary, $\text{SnO}_2(16)\text{@GO}$ senses lower VOC amounts (i.e. down to 0.1 ppm, Fig. 1e) evidencing, also in this case, a good linearity between signal intensities and ethanol concentrations (Fig. 1f, red line). However, with $\text{SnO}_2\text{-GO}$ 16:1 sample, a much more intense signal was recorded. Therefore, in this respect, the chemically prepared hybrid compound seems to be much more promising for the ethanol sensing.

Taking into account all these previous outcomes, the pivotal role of graphene oxide underneath metal oxide nanoparticles has been assessed and the controlled growth of tin dioxide revealed to be fundamental in order to achieve high sensitivity/good signal-to-noise ratio, even at lower operating temperatures. In particular, it has been demonstrated that sensor signal can be amplified by chemically coupling GO with the suitable amount of SnO_2 (so that an almost complete coverage of GO surface is obtained). This is probably due to the formation of a p-n heterojunction between graphene oxide (p-type [24]) and SnO_2 nanoparticles (n-type [25]). In particular, since the work functions of tin dioxide (annealed under oxygen stream) and GO are

5.7 eV [26] and 5.4 eV [27] respectively, the electrons tend to go more favorably from GO to SnO_2 , in order to equate the Fermi level. Hence, much more electrons are present in the conduction band of the metal oxide with respect to the pristine n-type semiconductor, and they can react with a greater amount of ambient oxygen molecules. Indeed, it is well known that the sensing mechanism is surface-controlled, i.e. the resistance change is affected by both species and amount of chemisorbed oxygen on semiconductors surface [28].

Besides, the exploitation of UV light has been reported to further help the metal oxide sensing capabilities [28,29]. When the UV radiation reaches the samples surface, photoactivated electrons are generated in the conduction band. Therefore, the optical excitation decreases the inter-grain barrier height, thereby increasing the free carriers density. As a result, the ambient oxygen molecules react more easily with the photoelectrons (e_{hv}^-), according to the following reactions:



The electrons, generated after the reaction with ethanol molecules, are released back to the metal oxide material thus leading to a decrease in the resistance. The improvement of sensor capability by means of UV light can be derived by the photoelectrons formation, which are much more highly reactive towards oxygen molecules [28,29].

Notably, all the adopted materials have shown quite fast response/recovery (about 70–90 s) towards ethanol (Table 1, 4th and 5th columns). However, the presence of graphene oxide seems to have further fastened (of around 10–20 s; Table 1, 4th and 5th columns) the sensing behavior, since the relative signals are sharper with respect to the pristine oxide ones (Fig. 1d).

Finally, some ethanol sensing results of graphene/metal oxide-based materials from the literature are summarized in Table 1. All the compounds of the present work exhibited excellent sensing performances, showing both very high sensitivities and response/recovery times comparable with the literature results.

3.2. Materials physico-chemical properties

To unravel the sensing mechanism underneath the composite materials behavior, several physico-chemical characterizations were performed.

Fig. 2a–c shows the structural properties by means of XRPD, FTIR and Raman spectroscopies. X-ray lines corroborate the effective synthesis of graphene oxide particles (Fig. 2a, grey line), through the shift of (0 0 2) plane of pure graphite to lower 2θ values (from 27° to 12° , the latter ascribable to the (0 0 1) reflection plane of GO). Moreover, by chemically controlling the growth of tin dioxide nanoparticles on GO compound, the achievement of a hybrid material showing a progressive coverage of graphene was obtained. Indeed, XRPD spectra reported in Fig. 2a have the characteristic peaks of cassiterite SnO_2 [30,31], even if some peaks broadening can be observed (especially for $\text{SnO}_2\text{-GO}$ 4:1 and 8:1), which is probably due to the presence of the below carbonaceous matrix. Actually, SnO_2 crystallites domain size is quite small for all the composite materials (from 5 nm of $\text{SnO}_2\text{-GO}$ 4:1 to 8 nm of $\text{SnO}_2\text{-GO}$ 16:1, Fig. 2a), thus underlining their low crystallinity.

Moreover, infrared and Raman spectroscopies have confirmed the successful accomplishment of the GO synthesis, by highlighting both the main stretching modes of C–O–C (around 1040 cm^{-1}), C=O (1715 cm^{-1}), C=C (1615 cm^{-1}) bonds (Fig. 2b), and the intensity rise of the ratio between the D and G Raman bands (Fig. 2c). Indeed, during the oxidation process, oxygen functional groups are introduced into the graphitic chain causing an increase of the D band intensity [32]. This is the reason why GO sample has a ratio more than three times higher (around 1.0) than the pristine graphite one (0.3). Going into detail, pure graphite displays the G and D bands at 1580 cm^{-1} and 1355 cm^{-1}

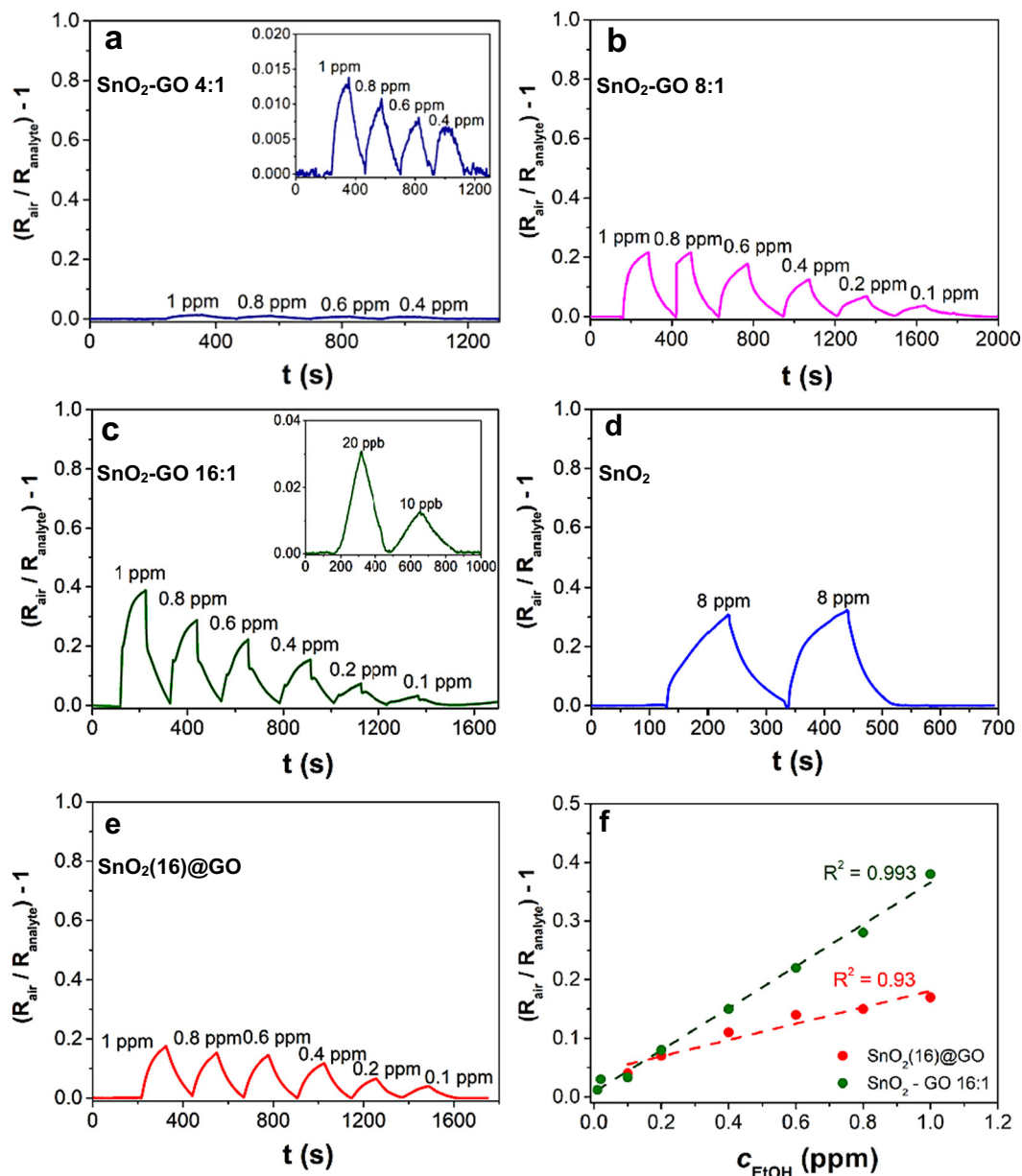


Fig. 1. (a–c) Ethanol sensor responses achieved by using hybrid SnO₂-GO 4:1, 8:1 and 16:1. For comparison, gas responses acquired with (d) pristine SnO₂ and (e) SnO₂(16)@GO (physically prepared) have been reported. All the tests were carried out in simulated air (80% N₂–20% O₂) at 150 °C, under UV light. (f) Linear correlation between sensors responses and ethanol concentration for SnO₂(16)@GO and SnO₂-GO 16:1 compounds.

respectively, corresponding to in-phase vibrations of the graphite lattice and its edges disorder [33,34] (Fig. 2c). Instead, the GO peaks are at 1310 cm⁻¹ (typically assigned to defects and disarranged structures of

the GO lattice [20,35]) and at 1605 cm⁻¹ (ascribable to the G band related to the vibration of sp²-bonded carbon atoms in the hexagonal lattice [20,35]). Furthermore, the controlled growth of SnO₂

Table 1

Comparison of ethanol sensing literature data through metal oxide/graphene materials-based sensors.

Material	Working temperature (°C)	Ethanol concentration	Response time (s)	Recovery time (s)	Reference
RGO-SnO ₂ nanocomposite	300	100 ppm	11	–	[49]
0.1 wt% GO/SnO ₂ nanocomposite	150	1000 ppm	30	–	[50]
Pd/SnO ₂ /graphene	150	2% in N ₂ inert gas	30	15	[51]
SnO ₂ nanosheets <i>via</i> GO-assisted hydrothermal route	250	100 ppm	9	457	[52]
SnO ₂ -RGO composites	300	2 ppm	5	9	[53]
Pure SnO ₂	150	8 ppm (UV light)	85	90	This work
SnO ₂ -GO 4:1	150	1 ppm (UV light)	77	80	This work
SnO ₂ -GO 8:1	150	1 ppm (UV light)	72	77	This work
SnO ₂ -GO 16:1	150	1 ppm (UV light)	70	75	This work
	RT	1 ppm (UV light)	310	320	This work

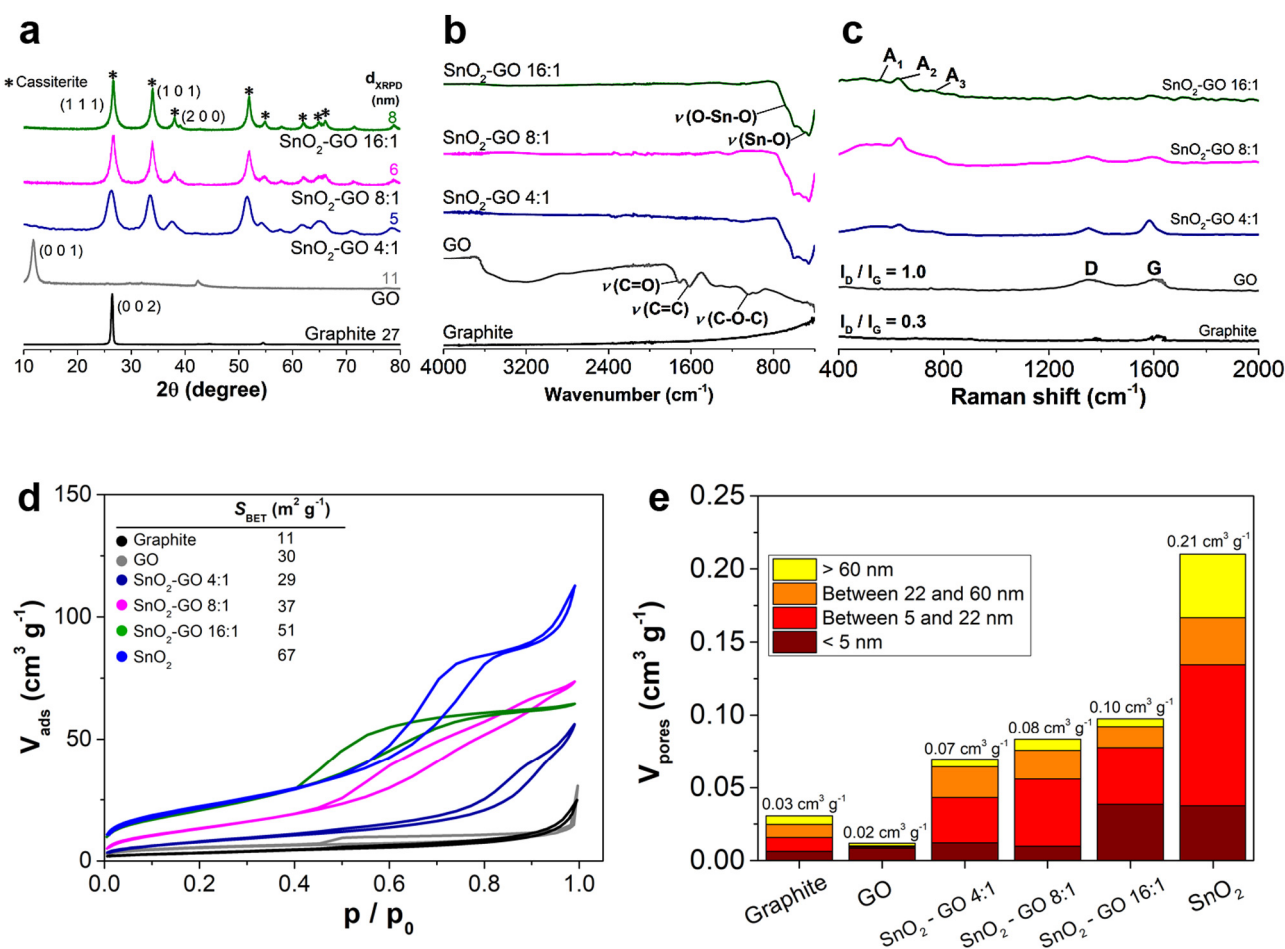


Fig. 2. Structural properties by (a) XRPD, (b) FTIR and (c) Raman spectroscopies results relative to graphite, graphene oxide and hybrid SnO₂-GO samples. (d) BET isotherms along with surface area values (S_{BET} in inset) and (e) histograms showing pores volume distribution for graphite, GO, pristine SnO₂ and hybrid SnO₂-GO compounds.

nanoparticles on the GO surface was confirmed by the appearance of A₁ (478 cm⁻¹), A₂ (624 cm⁻¹) and A₃ (766 cm⁻¹) peaks (Fig. 2c), typical of pure tin dioxide [36]. With this technique, the presence of GO can be highlighted in all the SnO₂-GO hybrid samples, since small traces of the D and G bands are observable and they gradually reduce passing from SnO₂-GO 4:1 (Fig. 2c, blue spectrum) to 16:1 material (Fig. 2c, green spectrum).

In order to increase the sensing capabilities, the surface properties (such as the active surface area and the porosity) should be evaluated. Concerning the former parameter, pristine graphite S_{BET} is about 11 m² g⁻¹ (inset Fig. 2d), in accordance to the reported literature [37]. After the oxidation/exfoliation process, the surface value has slightly increased (30 m² g⁻¹). Notwithstanding this parameter should be much higher (about 500 m² g⁻¹ [38]), the obtained value could be explained since GO interlayer spaces are often inaccessible to N₂ molecules in a few-layered GO structure, thus underestimating the real active surface area [39]. Furthermore, the shape of the hysteresis loop has two distinctive behaviors: *i*) the adsorption branch resembles a type II isotherm, in which the thickness of the adsorbed multilayer (at higher relative pressure) generally appears to increase without limit, when p/p_0 tends to 1; *ii*) the hysteresis loop is typical of type IV isotherm and could be explained by condensation of nitrogen molecules into mesopores that exceeds a certain critical width [40]. This type of isotherm is related to aggregates of platelet-like particles giving rise to slit-shaped pores [41] with an average pore diameter below 5 nm (as reported in Fig. 2e). In addition, the total pores volume decreases upon oxidation, indeed GO possesses a total volume around 40% lower than the

graphite one (Fig. 2e). By growing SnO₂ particles on GO sheets, S_{BET} slightly increased (from 29 m² g⁻¹ of SnO₂-GO 4:1 to 51 m² g⁻¹ of SnO₂-GO 16:1) reaching a value quite close to the surface area of the pristine SnO₂ (67 m² g⁻¹). Furthermore, also the total pores volume resembles the same trend, *i.e.* the presence of SnO₂ led to a rise of the volume, becoming close to the pristine tin dioxide, along with an increase of the percentage of particles with diameter higher than 60 nm (Fig. 2e).

Figs. 3 and S2 show the powders surface texture. In particular, SEM micrographs corroborate the fabrication of GO sheets (Fig. S2a and b), while micrometric aggregates (~50 μm or higher) have been observed for the hybrid SnO₂-GO samples (Fig. S2c–e). Once again, by transmission electron microscopy, both graphite and graphene oxide showed a layered structure (Fig. 3a and b). Specifically, for the former, the interlayer distance for (0 0 2) planes has been evaluated to be between 3.33 Å and 3.35 Å (by SAED, inset of Fig. 3a). As regards the SnO₂-GO hybrid compounds, spherical particles (typical of the pristine oxide, Fig. 3c) from around 5–10 nm up to 20 nm can be observed (by increasing the SnO₂ content, Fig. 3f), in accordance with XRPD results. Furthermore, the main diffraction planes ascribable to cassiterite polymorph can be identified in the corresponding SAED map (insets of Fig. 3d–f), with an interlayer distance of 3.32 Å for (1 1 0) and 2.64 Å for (2 0 0). Notably, in each SnO₂-GO material, the graphene presence underneath the metal oxide nanoparticles has been assessed evidencing the effective preservation of GO after the annealing step, thanks to the SnO₂ growth on its surface.

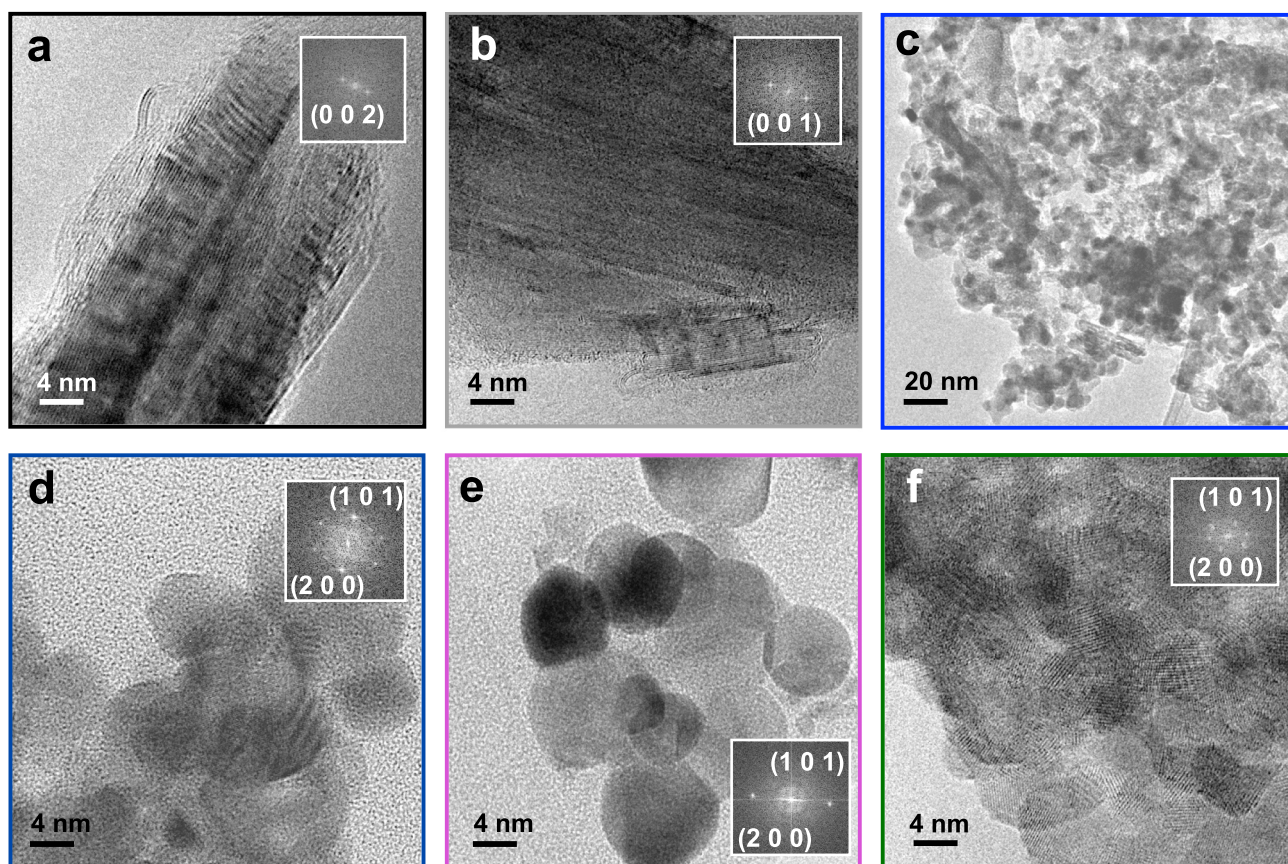


Fig. 3. TEM images of (a) graphite, (b) GO, (c) pristine SnO_2 , (d–f) composite SnO_2 -GO 4:1, 8:1 and 16:1 particles, respectively (insets: SAED images of the main phases diffraction planes).

3.3. Materials electrochemical characterization

The characteristic functional groups present on the surface of the graphene oxide have been deeply investigated by cyclic voltammetric measurements. Indeed, GO is intrinsically electroactive since its great amount of oxygen functionalities can be electrochemically oxidized and reduced. Therefore, CV may be used to determine the nature of these oxygen-containing groups. As reported by Pumera et al., by scanning the potentials from the negative (down to -2.0 V) to the positive (up to $+2.0$ V) values, peroxy, aldehydic, epoxy and carbonyl groups can be assessed [42]. Particularly, the GO reduction begins at about -1.0 V with two identifiable peaks (*i.e.* -1.0 and -2.0 V) which may be related to aldehyde and carbonyl groups, respectively (Fig. 4a) [42]. However, these reduction peaks could be only observed during the initial reduction (Fig. 4a, dark grey line). Moreover, by further scanning the reductive sweep, two other peaks could be observed at around -0.7 and -1.5 V, ascribable to two other oxygen-containing moieties (*i.e.* peroxy and epoxy groups) (Fig. 4a, light grey line) [42].

Once electrochemically investigated the surface chemistry of the graphene oxide material, CV measurements have been carried out by using differently modified-glassy carbon electrodes (by pristine SnO_2 , $\text{SnO}_2(16)\text{@GO}$ and $\text{SnO}_2\text{-GO}$ 16:1, the last due to its superior sensing capabilities), in the presence of a positively charged outer-sphere electrochemical probe (*i.e.* hexamine ruthenium (III) chloride, $[\text{Ru}(\text{NH}_3)_6]\text{Cl}_3$; Fig. 4b). By scanning the potentials in the cathodic direction, an interesting observation can be made. Actually, the reductive sweep shows two diverse behaviors: *i*) a defined peak-shaped curve in the case of GO, pristine SnO_2 and $\text{SnO}_2(16)\text{@GO}$ materials (at around -0.3 V); *ii*) a tendency to step-shaped curve for the hybrid $\text{SnO}_2\text{-GO}$ 16:1 (see Fig. 4b). This difference has been better highlighted by calculating the first derivative of the CV curves, which are reported in Fig.

S3. Actually, by focusing on the potential range between -0.25 and -0.50 V, only $\text{SnO}_2\text{-GO}$ 16:1 shows a completely flat behavior. From these experimental evidences, it may be inferred that the contribution of convergent diffusion seems to become predominant [43] in the case of this composite material, with respect to either pristine SnO_2 or mixed $\text{SnO}_2(16)\text{@GO}$ (insets of Fig. 4b). The growth of tin oxide on the graphene oxide sheets by forming catalytic isles, almost widely spaced, guarantees their independency in the experimental timescale and thus promotes convergent diffusion, already visible also with an outer-sphere probe [44]. The predominance of convergent diffusion allows obtaining higher sensitivities and low detection limits, thanks to high faradaic and low capacitive currents [45–48], important features of more performing sensors.

Therefore, in order to test the device performances towards real analytes, ethanol adsorption and detection onto powders modified-glassy carbon electrodes have been evaluated. Specifically, pure liquid ethanol was added to PBS electrolyte to have a final concentration of 1 mM. In the case of pristine SnO_2 , the addition of the alcohol molecules has no influence (as shown in the relative cyclic voltammograms; Fig. 4c, blue curves) remaining similar to the background, thus indicating that no observable electroactivity is detected for the molecule on this electrode material. The situation is different for $\text{SnO}_2(16)\text{@GO}$ sample (Fig. 4c, red curves), where in the background we can observe, as expected, the typical graphene peaks (see Fig. 4a) that disappear after ethanol addition. This is probably due to the analyte adsorption on the functional groups of GO, therefore irreversibly blocking their electrochemical reactions. On the other hand, the presence of SnO_2 has no effect, as demonstrated in the case of pure tin dioxide, and only the electrochemistry of graphene is observable. On the contrary, in the case of the hybrid material $\text{SnO}_2\text{-GO}$ 16:1, after ethanol addition we can observe the increase of the oxidation current with respect to the

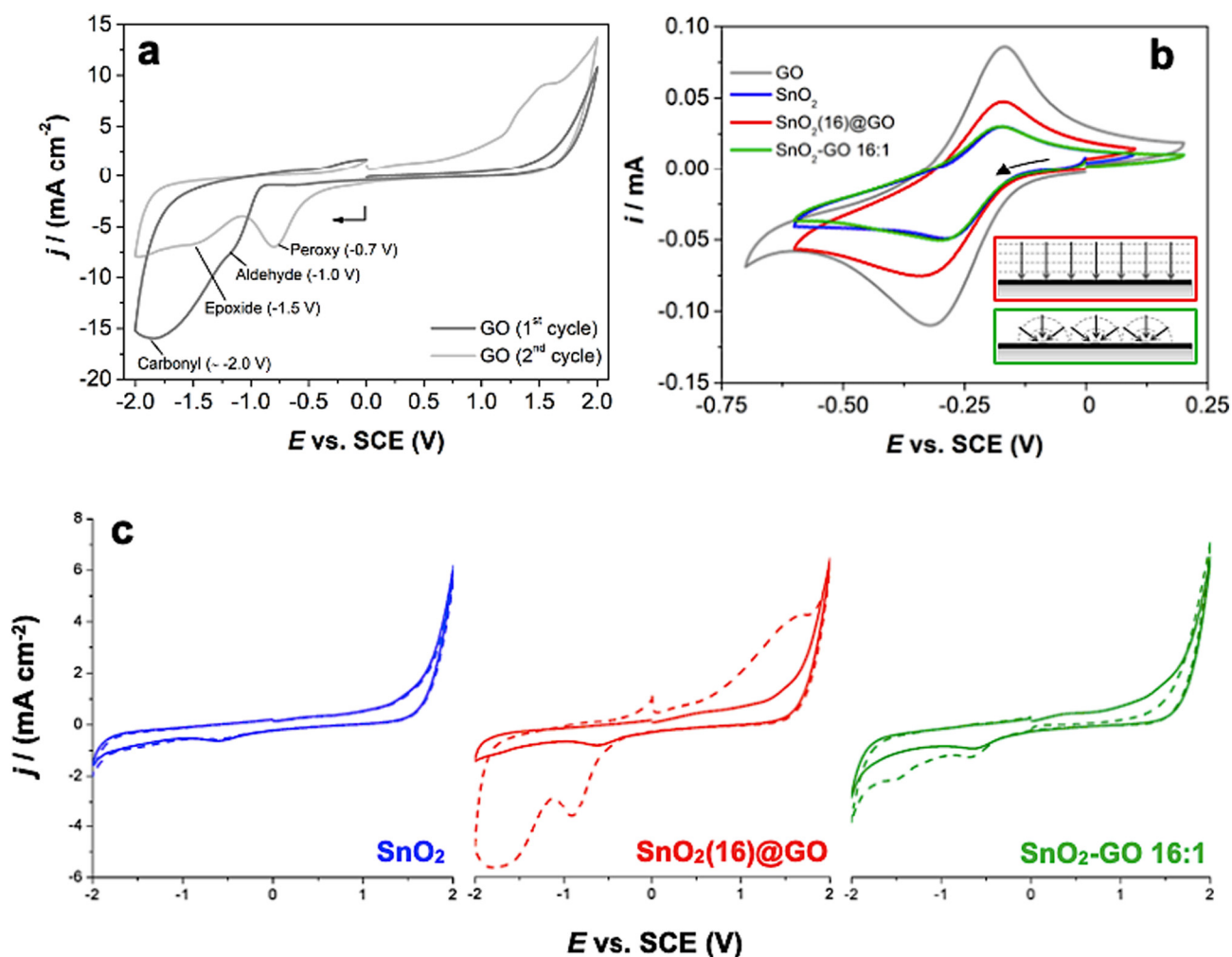


Fig. 4. (a) Cyclic voltammograms of bare and GO-modified glassy carbon. (b) Cyclic voltammograms relative to both bare and modified glassy carbon in the presence of 3 mM $[\text{Ru}(\text{NH}_3)_6]\text{Cl}_3$ probe. Inset: sketches of planar (red contour) and convergent (green contour) diffusion. (c) Cyclic voltammograms obtained with modified glassy carbon in the absence (dotted line) and presence (continuous line) of 1 mM ethanol. All the tests were conducted in 0.1 M PBS electrolyte, scan rate: 100 mV s^{-1} .

background (Fig. 4c, green curves), pointing out that ethanol can be detected at positive potentials. Moreover, since the majority of the graphene functional groups are occupied by SnO_2 nanoparticles, the irreversible adsorption of the analyte is prevented.

Hence, starting from these significant electrochemical outcomes, the improvement of the gaseous ethanol sensing by $\text{SnO}_2\text{-GO 16:1}$ material could be further corroborated and deeply explained as the result of the synergistic effect between graphene oxide and tin dioxide. Moreover, by performing the sensing tests at positive potentials (*i.e.* +1.0 V), the ethanol detection was favored especially for $\text{SnO}_2\text{-GO 16:1}$ sample, as demonstrated by CV measurements.

4. Conclusions

Herein, we develop a novel hybrid material based on graphene oxide/tin dioxide compounds exhibiting superior sensing behavior towards ethanol at temperatures (*i.e.* 150 °C and room temperature) lower than the usual operating ones (> 300 °C), by exploiting the UV light. In order to give a satisfying explanation behind the improvement of the sensing behavior, several composites with different SnO_2/GO ratios (4:1, 8:1 and 16:1) were tailored synthesized, showing the effective nano- SnO_2 coverage onto GO surfaces. The greatest response was achieved with the highest content of tin oxide (*i.e.* $\text{SnO}_2\text{-GO 16:1}$), both at 150 °C and room temperature, being able to detect very low ethanol

concentrations (10 ppb, 0.6 ppm at 150 and 25 °C, respectively).

Hence, we demonstrated that the almost coverage of graphene oxide sheets by SnO_2 can enhance the sensing features thanks to: *i*) the formation of a $p(\text{GO}) - n(\text{SnO}_2)$ heterojunction that induces electrons to pass from GO to SnO_2 conduction band; *ii*) the resulting greater amount of adsorbed oxygen species, which react with the target ethanol molecules; and *iii*) the increased electron transfer, due to the formation of widely spaced isles of the metal oxide on the carbonaceous material (*i.e.* favoring convergent diffusion).

Furthermore, for the sake of clarity, chemically synthesized $\text{SnO}_2\text{-GO 16:1}$ was compared to pure SnO_2 and the corresponding mechanically prepared ($\text{SnO}_2(16)\text{@GO}$) compound. Notably, $\text{SnO}_2(16)\text{@GO}$ showed worse sensing features with respect to the homologous $\text{SnO}_2\text{-GO 16:1}$. This fact is probably ascribable to the occurrence of either a more intimate contact between GO and SnO_2 , when chemically synthesized, or to the growth of widely spaced metal oxide isles. Moreover, through CV measurements, we evidenced that ethanol can be more easily detected at positive potentials, especially in the case of the hybrid $\text{SnO}_2\text{-GO 16:1}$.

Hence, we believe that the peculiar properties of the as-synthesized compound could set the basis for the development of novel hybrid materials that may be applied in the gas sensing field.

Conflict of interest

The authors declare that there is no conflict of interest regarding the publication of this paper.

Acknowledgments

The authors gratefully acknowledge Dr. Maria Carmen Valsania, Dipartimento di Chimica and NIS, Inter-department Center, Università di Torino; Prof. Saveria Santangelo, Dipartimento di Ingegneria Civile, dell'Energia, dell'Ambiente e dei Materiali, Università Mediterranea di Reggio Calabria; and Prof. Salvatore Patanè, Dipartimento di Scienze Matematiche e Informatiche, Scienze Fisiche e Scienze della Terra, Università degli Studi di Messina for some data acquisition and their relative interpretation.

A.T. gratefully acknowledges the support of the Australian Research Council DP150101939, the Australian Research Council DE160100569 and the Westpac2016 Research Fellowship.

Appendix A. Supplementary data

Table S1: Sn/C atomic ratios calculated from XPS surveys for hybrid materials; Fig. S1: Room temperature ethanol sensor responses obtained by hybrid SnO₂-GO 4:1, 8:1, 16:1; Fig. S2: SEM micrographs of (a) graphite, (b) GO, (c) pristine SnO₂, (d–f) hybrid SnO₂-GO 4:1, 8:1 and 16:1 samples; Fig. S3: First derivative of the CV current cathodic branch for pristine SnO₂, SnO₂(16)@GO and SnO₂-GO 16:1. Supplementary data to this article can be found online at doi:<https://doi.org/10.1016/j.apsusc.2019.04.046>.

References

- M.-R. Yu, G. Suyambakasam, R.-J. Wu, M. Chavali, Performance evaluation of ZnO–CuO hetero junction solid state room temperature ethanol sensor, *Mater. Res. Bull.* 47 (2012) 1713–1718. doi:10.1016.
- Y. He, P. Tang, J. Li, J. Zhang, F. Fan, D. Li, Ultrafast response and recovery ethanol sensor based on SnO₂ quantum dots, *Mater. Lett.* 165 (2016) 50–54. <https://doi.org/10.1016/j.matlet.2015.11.092>.
- M. NaderiNasrabadi, Y. Mortazavi, A.A. Khodadadi, Highly sensitive and selective Gd₂O₃-doped SnO₂ ethanol sensors synthesized by a high temperature and pressure solvothermal method in a microreactor, *Sensors Actuators B Chem.* 230 (2016) 130–139. doi:10.1016.
- W. Li, X. Wu, N. Han, J. Chen, X. Qian, Y. Deng, W. Tang, Y. Chen, MOF-derived hierarchical hollow ZnO nanocages with enhanced low-concentration VOCs gas-sensing performance, *Sensors Actuators B Chem.* 225 (2016) 158–166. <https://doi.org/10.1016/j.snb.2015.11.034>.
- W. Li, S. Ma, Y. Li, G. Yang, Y. Mao, J. Luo, D. Gengzang, X. Xu, S. Yan, Chemical enhanced ethanol sensing performance of hollow ZnO-SnO₂ core-shell nanofibers, *Sensors Actuators B Chem.* 211 (2015) 392–402. <https://doi.org/10.1016/j.snb.2015.01.090>.
- Z. Song, Z. Wei, B. Wang, Z. Luo, S. Xu, W. Zhang, H. Yu, M. Li, Z. Huang, J. Zang, F. Yi, H. Liu, Sensitive Room-Temperature H₂S Gas Sensors Employing SnO₂ Quantum Wire/Reduced Graphene Oxide Nanocomposites, (2016). <https://doi.org/10.1021/acs.chemmater.5b04850>.
- M. Righettoni, A. Tricoli, S. Gass, A. Schmid, A. Amann, S.E. Pratsinis, Breath acetone monitoring by portable Si:WO₃ gas sensors, *Anal. Chim. Acta* 738 (2012) 69–75. <https://doi.org/10.1016/j.aca.2012.06.002>.
- M. Righettoni, A. Tricoli, S.E. Pratsinis, Si:WO₃ sensors for highly selective detection of acetone for easy diagnosis of diabetes by breath analysis, *Anal. Chem.* 82 (2010) 3581–3587. <https://doi.org/10.1021/ac902695n>.
- E. Wongrat, N. Chanlek, C. Chueaiarrom, B. Samransuksamer, N. Hongsith, S. Choopun, Low temperature ethanol response enhancement of ZnO nanostructures sensor decorated with gold nanoparticles exposed to UV illumination, *Sensors Actuators A Phys.* 251 (2016) 188–197. <https://doi.org/10.1016/j.sna.2016.10.022>.
- X. Kou, N. Xie, F. Chen, T. Wang, L. Guo, C. Wang, Q. Wang, J. Ma, Y. Sun, H. Zhang, G. Lu, Superior acetone gas sensor based on electrospun SnO₂ nanofibers by Rh doping, *Sensors Actuators B Chem.* 256 (2018) 861–869. <https://doi.org/10.1016/j.snb.2017.10.011>.
- J. Li, P. Tang, J. Zhang, Y. Feng, R. Luo, A. Chen, D. Li, Facile synthesis and acetone sensing performance of hierarchical SnO₂ hollow microspheres with controllable size and shell thickness, *Ind. Eng. Chem. Res.* 55 (2016) 3588–3595. <https://doi.org/10.1021/acs.iecr.6b00060>.
- A.M.K. Janghorban, B.H.G. Neri, Metal-core@metal oxide-shell nanomaterials for gas-sensing applications: a review, *J. Nanopart. Res.* 17 (2015) 1–36. <https://doi.org/10.1007/s11051-015-3164-5>.
- H.J. Kim, J.H. Lee, Highly sensitive and selective gas sensors using p-type oxide semiconductors: overview, *Sensors Actuators B Chem.* 192 (2014) 607–627. <https://doi.org/10.1016/j.snb.2013.11.005>.
- S. Gupta Chatterjee, S. Chatterjee, A.K. Ray, A.K. Chakraborty, Graphene-metal oxide nanohybrids for toxic gas sensor: a review, *Sensors Actuators B Chem.* 221 (2015) 1170–1181. <https://doi.org/10.1016/j.snb.2015.07.070>.
- H.W. Kim, Y.J. Kwon, A. Mirzaei, S.Y. Kang, M.S. Choi, J.H. Bang, S.S. Kim, Synthesis of zinc oxide semiconductors-graphene nanocomposites by microwave irradiation for application to gas sensors, *Sensors Actuators B Chem.* 249 (2017) 590–601. <https://doi.org/10.1016/j.snb.2017.03.149>.
- S.S. Varghese, S.H. Varghese, S. Swaminathan, K.K. Singh, V. Mittal, Two-dimensional materials for sensing: graphene and beyond, (2015) 651–687. doi:<https://doi.org/10.3390/electronics4030651>.
- H. Zhang, Y. Cen, Y. Du, S. Ruan, Enhanced acetone sensing characteristics of ZnO/graphene composites, *Sensors (Switzerland)* 16 (2016) 1–10. <https://doi.org/10.3390/s16111876>.
- R. Kalidoss, S. Umopathy, Y. Sivalingam, An investigation of GO-SnO₂-TiO₂ ternary nanocomposite for the detection of acetone in diabetes mellitus patient's breath, *Appl. Surf. Sci.* 449 (2018) 677–684. <https://doi.org/10.1016/j.apsusc.2017.12.090>.
- C. Botas, P. Álvarez, P. Blanco, M. Granda, C. Blanco, R. Santamaría, L.J. Romasanta, R. Verdejo, M.A. López-Manchado, R. Menéndez, Graphene materials with different structures prepared from the same graphite by the Hummers and Brodie methods, *Carbon N. Y.* 65 (2013) 156–164. <https://doi.org/10.1016/j.carbon.2013.08.009>.
- J. Chen, B. Yao, C. Li, G. Shi, An improved Hummers method for eco-friendly synthesis of graphene oxide, *Carbon N. Y.* 64 (2013) 225–229. <https://doi.org/10.1016/j.carbon.2013.07.055>.
- L. Bonizzoni, S. Bruni, A. Galli, M. Gargano, V. Guglielmi, N. Ludwig, L. Lodi, M. Martini, Non-invasive in situ analytical techniques working in synergy: the application on gradials held in the Certosa di Pavia, *Microchem. J.* 126 (2016) 172–180. <https://doi.org/10.1016/j.microc.2015.12.001>.
- R. Bo, N. Nasiri, H. Chen, D. Caputo, L. Fu, A. Tricoli, Low-voltage high-performance UV photodetectors: an interplay between grain boundaries and debye length, *ACS Appl. Mater. Interfaces* 9 (2017) 2606–2615. <https://doi.org/10.1021/acsami.6b12321>.
- M. Righettoni, A. Tricoli, S.E. Pratsinis, Thermally stable, silica-doped e-WO₃ for sensing of acetone in the human breath, *Chem. Mater.* 22 (2010) 3152–3157. <https://doi.org/10.1021/cm1001576>.
- D.T. Phan, G.S. Chung, P-n junction characteristics of graphene oxide and reduced graphene oxide on n-type Si(111), *J. Phys. Chem. Solids* 74 (2013) 1509–1514. <https://doi.org/10.1016/j.jpccs.2013.02.007>.
- L. Jin, W. Chen, H. Zhang, G. Xiao, C. Yu, Q. Zhou, Characterization of reduced graphene oxide (rGO)-loaded SnO₂ nanocomposite and applications in C₂H₂ gas detection, *Appl. Sci.* 7 (2016) 19. <https://doi.org/10.3390/app7010019>.
- A. Klein, C. Körber, A. Wachau, F. Säuberlich, Y. Gassenbauer, R. Schafranek, S.P. Harvey, T.O. Mason, Surface potentials of magnetron sputtered transparent conducting oxides, *Thin Solid Films* 518 (2009) 1197–1203. <https://doi.org/10.1016/j.tsf.2009.05.057>.
- L. Sygellou, S. Paterakis, C. Galiotis, D. Tasis, Work function tuning of reduced graphene oxide thin films, *J. Phys. Chem. C* 120 (2016) 281–290. <https://doi.org/10.1021/acs.jpcc.5b09234>.
- P. Zhang, G. Pan, B. Zhang, J. Zhen, Y. Sun, High sensitivity ethanol gas sensor based on Sn-doped ZnO under visible light irradiation at low temperature, *Mater. Res.* 17 (2014) 817–822. <https://doi.org/10.1590/1516-1439.235713>.
- Z.Q. Zheng, J.D. Yao, B. Wang, G.W. Yang, Light-controlling, flexible and transparent ethanol gas sensor based on ZnO nanoparticles for wearable devices, *Sci. Rep.* 5 (2015) 1–8. <https://doi.org/10.1038/srep11070>.
- S. Ardizzone, C.L. Bianchi, L. Borgese, G. Cappelletti, C. Locatelli, A. Minguzzi, S. Rondinini, A. Vertova, P.C. Ricci, C. Cannas, A. Musinu, Physico-chemical characterization of IrO₂-SnO₂ sol-gel nanopowders for electrochemical applications, *J. Appl. Electrochem.* 39 (2009) 2093–2105. <https://doi.org/10.1007/s10800-009-9895-1>.
- A. Kumar, L. Rout, L.S.K. Achary, A. Mohanty, R.S. Dhaka, P. Dash, An investigation into the solar light-driven enhanced photocatalytic properties of a graphene oxide-SnO₂-TiO₂ ternary nanocomposite, *RSC Adv.* 6 (2016) 32074–32088. <https://doi.org/10.1039/C6RA02067D>.
- H. Chen, X. Pu, M. Gu, J. Zhu, L. Cheng, Tailored synthesis of SnO₂@graphene nanocomposites with enhanced photocatalytic response, *Ceram. Int.* 42 (2016) 17717–17722. <https://doi.org/10.1016/j.ceramint.2016.08.095>.
- K.N. Kudin, B. Ozbas, H.C. Schniepp, R.K. Prud'homme, I.A. Aksay, R. Car, Raman spectra of graphite oxide and functionalized graphene sheets, *Nano Lett.* 8 (2008) 36–41. <https://doi.org/10.1021/nl071822y>.
- X. Díez-Betriu, S. Álvarez-García, C. Botas, P. Álvarez, J. Sánchez-Marcos, C. Prieto, R. Menéndez, A. De Andrés, Raman spectroscopy for the study of reduction mechanisms and optimization of conductivity in graphene oxide thin films, *J. Mater. Chem. C* 1 (2013) 6905–6912. <https://doi.org/10.1039/c3tc31124d>.
- E.T. Mombeshora, P.G. Ndungu, V.O. Nyamori, Effect of graphite/sodium nitrate ratio and reaction time on the physicochemical properties of graphene oxide, *New Carbon Mater* 32 (2017) 174–187. [https://doi.org/10.1016/S1872-5805\(17\)60114-8](https://doi.org/10.1016/S1872-5805(17)60114-8).
- J. Zuo, C. Xu, X. Liu, C. Wang, C. Wang, Y. Hu, Y. Qian, Study of the Raman spectrum of nanometer SnO₂, *J. Appl. Phys.* 75 (1994) 1835–1836. <https://doi.org/10.1063/1.356348>.
- M.P. Trammell, P.J. Pappano, Analysis of Natural Graphite, Synthetic Graphite, and Thermosetting Resin Candidates for Use in Fuel Compact Matrix, (2011), pp. 1–66.

- <https://doi.org/10.2172/1024284>.
- [38] S. Stankovich, D.A. Dikin, R.D. Piner, K.A. Kohlhaas, A. Kleinhammes, Y. Jia, Y. Wu, S.B.T. Nguyen, R.S. Ruoff, Synthesis of graphene-based nanosheets via chemical reduction of exfoliated graphite oxide, *Carbon N. Y.* 45 (2007) 1558–1565, <https://doi.org/10.1016/j.carbon.2007.02.034>.
- [39] T. Szabó, E. Tombácz, E. Illés, I. Dékány, Enhanced acidity and pH-dependent surface charge characterization of successively oxidized graphite oxides, *Carbon N. Y.* 44 (2006) 537–545, <https://doi.org/10.1016/j.carbon.2005.08.005>.
- [40] T. Gao, W. Xu, L. Gong, Z. Wang, Z. Yang, Y. Song, Y. Xiong, Folded three-dimensional graphene with uniformly distributed mesopores for high-performance supercapacitors, *RSC Adv.* 5 (2015) 33767–33771, <https://doi.org/10.1039/c5ra02991k>.
- [41] K.S.W. Sing, D.H. Everett, R.A.W. Haul, L. Moscou, R.S. Pierotti, J. Rouquerol, T. Siemienińska, International union of pure commission on colloid and surface chemistry including catalysis-reporting physisorption data for gas/solid systems with special reference to the determination of surface area and porosity, *Pure Appl. Chem.* 57 (1985) 603–619, <https://doi.org/10.1351/pac198557040603>.
- [42] A.Y.S. Eng, A. Ambrosi, C.K. Chua, F. Šaněk, Z. Sofer, M. Pumera, Unusual inherent electrochemistry of graphene oxides prepared using permanganate oxidants, *Chem. - A Eur. J.* 19 (2013) 12673–12683, <https://doi.org/10.1002/chem.201301889>.
- [43] Compton, Banks, Understanding voltammetry.
- [44] C. Ingrosso, G.V. Bianco, V. Pifferi, P. Guffanti, F. Petronella, R. Comporelli, A. Agostiano, M. Striccoli, I. Palchetti, L. Falciola, M.L. Curri, G. Bruno, Enhanced photoactivity and conductivity in transparent TiO₂ nanocrystals/graphene hybrid anodes, *J. Mater. Chem. A* 5 (2017) 9307–9315, <https://doi.org/10.1039/c7ta01425b>.
- [45] G. Herzog, V. Beni, Stripping voltammetry at micro-interface arrays: a review, *Anal. Chim. Acta* 769 (2013) 10–21, <https://doi.org/10.1016/j.aca.2012.12.031>.
- [46] G. Soliveri, V. Pifferi, G. Panzarasa, S. Ardizzone, G. Cappelletti, D. Meroni, K. Sparnacci, L. Falciola, Self-cleaning properties in engineered sensors for dopamine electroanalytical detection, *Analyst* 140 (2015) 1486–1494, <https://doi.org/10.1039/C4AN02219J>.
- [47] A.O. Simm, S. Ward-Jones, C.E. Banks, R.G. Compton, Novel methods for the production of silver microelectrode-arrays: their characterisation by atomic force microscopy and application to the electro-reduction of halothane, *Anal. Sci.* 21 (2005) 667–671, <https://doi.org/10.2116/analsci.21.667>.
- [48] S. Daniele, M. Baldo, C. Bragato, Recent developments in stripping analysis on microelectrodes, *Curr. Anal. Chem.* 4 (2008) 215–228, <https://doi.org/10.2174/157341108784911343>.
- [49] C.A. Zito, T.M. Perfecto, D.P. Volanti, Impact of reduced graphene oxide on the ethanol sensing performance of hollow SnO₂ nanoparticles under humid atmosphere, *Sensors Actuators B Chem.* 244 (2017) 466–474, <https://doi.org/10.1016/j.snb.2017.01.015>.
- [50] M. Arvani, H. Mohammad Aliha, A.A. Khodadadi, Y. Mortazavi, Graphene oxide/SnO₂ nanocomposite as sensing material for breathalyzers: selective detection of ethanol in the presence of automotive CO and hydrocarbons emissions, *Sci. Iran. O* (0) (2017) 0, <https://doi.org/10.24200/sci.2017.4350>.
- [51] S. Dhall, M. Kumar, M. Bhatnagar, B.R. Mehta, Dual gas sensing properties of graphene-Pd/SnO₂ composites for H₂ and ethanol: role of nanoparticles-graphene interface, *Int. J. Hydrog. Energy* 43 (2018) 17921–17927, <https://doi.org/10.1016/j.ijhydene.2018.07.066>.
- [52] C. Zhao, H. Gong, W. Lan, R. Ramachandran, H. Xu, S. Liu, F. Wang, Facile synthesis of SnO₂ hierarchical porous nanosheets from graphene oxide sacrificial scaffolds for high-performance gas sensors, *Sensors Actuators B Chem.* 258 (2018) 492–500, <https://doi.org/10.1016/j.snb.2017.11.167>.
- [53] Y. Chang, Y. Yao, B. Wang, H. Luo, T. Li, L. Zhi, Reduced graphene oxide mediated SnO₂ nanocrystals for enhanced gas-sensing properties, *J. Mater. Sci. Technol.* 29 (2013) 157–160, <https://doi.org/10.1016/j.jmst.2012.11.007>.